



RESEARCH ARTICLE

# Third-harmonic generation via rapid adiabatic passage based on gradient deuterium $\text{KD}_x\text{H}_{2-x}\text{PO}_4$ crystal

Lailin Ji<sup>1,†</sup>, Li Yin<sup>1,2,†</sup>, Jinsheng Liu<sup>1,†</sup>, Xianghe Guan<sup>1</sup>, Mingxia Xu<sup>3</sup>, Xun Sun<sup>3</sup>, Dong Liu<sup>1</sup>, Hao Xu<sup>1</sup>, Ruijing He<sup>1</sup>, Tianxiong Zhang<sup>1</sup>, Wei Feng<sup>1</sup>, Yong Cui<sup>1</sup>, Xiaohui Zhao<sup>1</sup>, Yanqi Gao<sup>1</sup>, and Zhan Sui<sup>1</sup>

<sup>1</sup>Shanghai Institute of Laser Plasma, China Academy of Engineering Physics, Shanghai, China

<sup>2</sup>Key Laboratory on High Power Laser and Physics, Shanghai Institute of Optics and Fine Mechanics, Chinese Academy of Sciences, Shanghai, China

<sup>3</sup>State Key Laboratory of Crystal Materials, Shandong University, Jinan, China

(Received 27 September 2024; revised 11 November 2024; accepted 9 December 2024)

## Abstract

Broadband frequency-tripling pulses with high energy are attractive for scientific research, such as inertial confinement fusion, but are difficult to scale up. Third-harmonic generation via nonlinear frequency conversion, however, remains a trade-off between bandwidth and conversion efficiency. Based on gradient deuterium deuterated potassium dihydrogen phosphate ( $\text{KD}_x\text{H}_{2-x}\text{PO}_4$ , DKDP) crystal, here we report the generation of frequency-tripling pulses by rapid adiabatic passage with a low-coherence laser driver facility. The efficiency dependence on the phase-matching angle in a Type-II configuration is studied. We attained an output at 352 nm with a bandwidth of 4.4 THz and an efficiency of 36%. These results, to the best of our knowledge, represent the first experimental demonstration of gradient deuterium DKDP crystal in obtaining frequency-tripling pulses. Our research paves a new way for developing high-efficiency, large-bandwidth frequency-tripling technology.

**Keywords:** DKDP crystal; nonlinear frequency conversion; rapid adiabatic passage; third-harmonic generation

## 1. Introduction

The third-harmonic generation (THG) source from Nd:glass laser driver facilities has become an ideal wavelength for inertial confinement fusion (ICF). Accurately, THG light sources in conjunction with broad bandwidth can effectively suppress laser plasma instability (LPI) issues<sup>[1,2]</sup>, making it crucial for the successful ignition of laser-driven ICF. Quadratic nonlinear frequency conversion, including second-harmonic generation (SHG) and sum-frequency generation (SFG), is a direct route for converting fundamental light pulses into the THG region<sup>[3,4]</sup>. Eimerl *et al.*<sup>[5]</sup> and Babushkin *et al.*<sup>[6]</sup> validated the two-crystal cascade scheme by SFG, achieving a THG bandwidth of up to 1.1 THz@351 nm. Dorrer *et al.*<sup>[7]</sup> proposed a novel method using grating angular dispersion compensation, combined

with broadband and narrowband SFG to achieve a THG bandwidth of 10 THz@351 nm. While these schemes have successfully generated broadband THG, the former is constrained by the THG efficiency, which is quite sensitive to the spacing between the two mixers, and the latter is limited by the damage threshold of ultraviolet gratings, making it difficult to widely promote application. Therefore, how to efficiently obtain broadband THG light sources with robustness is a crucial issue that needs to be addressed urgently.

Nonlinear frequency conversion, a widely used route for THG, however, faces a trade-off between bandwidth and conversion efficiency<sup>[8,9]</sup>. Essentially, it involves managing population numbers within an inhomogeneous quantum two-state system. The same issue also arises in quantum two-level systems with a global inhomogeneity: the nonuniform resonant frequency limits the complete population inversion or any alternative required quantum state preparation to a small part of the ensemble. The solution has long been established<sup>[10–12]</sup>: as for nuclear magnetic resonance and atoms or molecules, rapid adiabatic passage (RAP)<sup>[13]</sup> produces violent particle number inversion without precise

Correspondence to: L. Ji, Shanghai Institute of Laser Plasma, China Academy of Engineering Physics, Shanghai 201800, China. Email: jsy-cjll@siom.ac.cn

<sup>†</sup>These authors contributed equally to this work.

integration of power electromagnetic coupling pulses, effectively overcoming the impurities in the preparation of quantum states in nonuniform ensembles. Fortunately, it is noted that RAP in the parametric three-wave mixing process, analogous to the two-level quantum system, can overcome the trade-off and achieve high-efficiency frequency conversion with a broad bandwidth<sup>[14,15]</sup>. Here, the phase mismatch gradually varies from a significant negative (positive) to positive (negative) value as the interaction unfolds. The RAP system should ideally start and finish near a stationary state in which the nonlinear coupling is negligible, suggesting a robust performance.

The adiabatic THG process essentially involves the regulation of refractive index characteristics of the crystal to satisfy the RAP conditions<sup>[16]</sup>. The reported regulation methods mainly focus on the application of external fields, including temperature<sup>[17]</sup> and electric fields<sup>[18]</sup>. These two methods, however, are easily affected by external perturbations. One expected approach is to perform gradient-doping concentration inside the nonlinear crystal to modify its refractive index, thereby permanently altering the intrinsic properties of the crystal without external field control. In our previous theoretical work, we utilized gradient-doping crystals in the adiabatic THG process and formulated a comprehensive technical scheme. In this work, we present an experimental demonstration of a gradient-doped crystal in generating a frequency-tripling pulse through RAP by a nanosecond laser, which represents the current state of the art in this

field. A compact THG setup and a high-efficiency THG architecture were tested, respectively. The former achieved an efficiency of 7%, while the latter, which was equipped with a narrowband fundamental laser, reached an efficiency of 36%. These results demonstrate the superiority of RAP-based frequency-tripling in terms of incident angle tolerance, high efficiency and broad bandwidth.

## 2. Rapid adiabatic passage based on gradient deuterium deuterated potassium dihydrogen phosphate crystal

To date, with 1  $\mu\text{m}$  lasers, typical oxide crystals of  $\beta\text{-BaB}_2\text{O}_4$ <sup>[19,20]</sup>,  $\text{CsLiB}_6\text{O}_{10}$ <sup>[21,22]</sup>,  $\text{LiB}_3\text{O}_5$ <sup>[23,24]</sup> and  $\text{KH}_2\text{PO}_4$  (KDP)<sup>[25,26]</sup> have been widely applied in up- and down-frequency conversion. KDP crystals, notable for their capability to grow large-sized, high-quality single crystals, possess distinctive advantages in the THG process. It has been demonstrated that KDP can be extensively applied for THG driven by high-power lasers<sup>[27,28]</sup>. We intend to implement the gradient-doping strategy in KDP crystals and demonstrate its potential in THG.

In contrast to KDP with a fixed doping concentration, Hao *et al.*<sup>[29]</sup> from Shandong University have successfully grown KDP crystals doped with a gradient deuterium (Figure 1(a)) through a ‘point-seed’ rapid growth method in a 5 L container. Within the crystal, the deuterium concentration

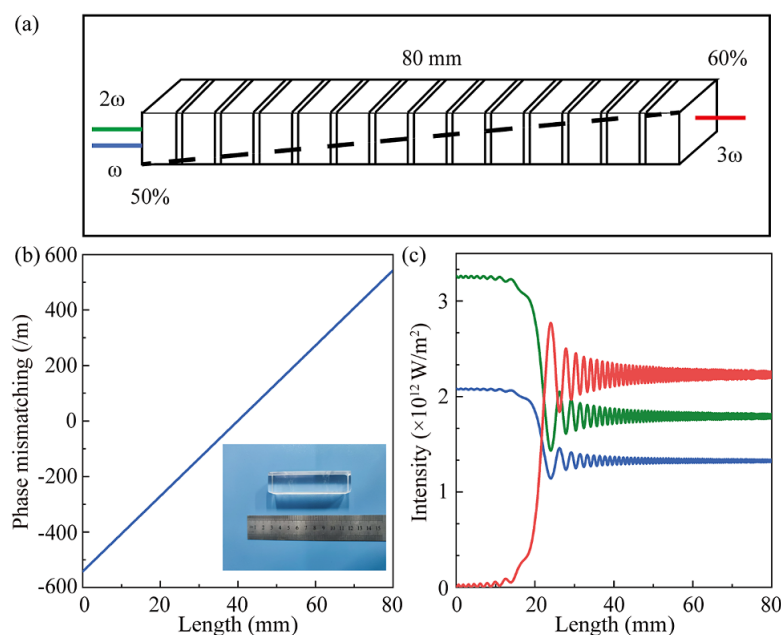


**Figure 1.** (a) Diagram of gradient deuterium DKDP. A high-quality Type-II PM direction gradient deuterium DKDP crystal with dimensions of 20 mm  $\times$  20 mm  $\times$  80 mm is employed in the THG scheme. The deuterium content ranges from 50% to 60% with a change of 10% in an 80-mm-thickness crystal and maintains 55% at the center of the crystal. (b) The variation of phase mismatch in SFG as a function of crystal length. The calculations assumed a monochromatic light of frequency mixing at 1058, 529 and 352 nm, respectively. Insert: photo of gradient deuterium DKDP crystal. (c) Intensity evolution for SFG of the fundamental frequency (blue) and second (green) and third (red) harmonics. The input broadband fundamental frequency light has an intensity of 0.8  $\text{GW/cm}^2$ . Assuming the total transmission loss before the KDP crystal is 20% and the efficiency of broadband SHG with KDP is 50%, the intensity broadband SHG is about  $3.2 \times 10^{12} \text{ W/m}^2$  and the given narrowband intensity is comparable to the SHG.

increases linearly along the beam propagation direction. The amount of doping deuterium directly affects the properties of the refractive index in KDP crystal, and the refractive index is varied with the doping deuterium given in the following formula:  $n^2(x) = xn_D^2 + (1-x)n_H^2$ , where  $n$  represents the refractive index of deuterium-doped crystal,  $n_D$  is the refractive index of fully doped deuterium,  $n_H$  corresponds to the refractive index of a deuterium-free KDP crystal and  $x$  denotes the doping deuterium along the optical axis.

Gradient deuterium deuterated potassium dihydrogen phosphate (DKDP) crystal has remarkable potential in high-efficiency THG wherein adiabatic schemes are especially attractive for their robustness to small changes in parameters that affect the phase evolution of the process. Analogous to adiabatic mechanism in two-level quantum systems, the phase mismatch parameter should vary slowly during the conversion process, from a large negative value to a large positive one or vice versa. In the presence of a sufficiently strong pump field, as for SFG, energy is efficiently converted from lower to higher frequency. Thus, the adiabatic scheme relaxes the restriction of minimizing the phase mismatch between the interacting beams, and instead requires  $\Delta k$  to be varied slowly during frequency conversion. The adiabatic conditions can be written as follows<sup>[30–32]</sup>:

$$\left| \frac{d\Delta k}{dz} \right| \ll \frac{(\Delta k^2 + \kappa^2)^{3/2}}{\kappa}, \quad (1)$$

where  $\Delta k = k_1 + k_2 - k_3$  represents the phase mismatch among the interacting waves,  $k_1$ ,  $k_2$  and  $k_3$  refer to the wave-number of the seed, pump and generated frequency, respectively,  $z$  is the position along the propagation direction,  $\kappa$  is the coupling coefficient and  $\kappa = \frac{4\pi w_1 w_3}{\sqrt{k_1 k_3} c^2} \chi^{(2)} A_2$ , where

$w_1$  and  $w_3$  are the frequencies of the seed and the generated sum frequency,  $c$  is the light speed in vacuum,  $A_2$  is the pump amplitude and  $\chi^{(2)}$  is the second-order susceptibility of the crystal.

The violent phase mismatch within the crystal, near the entrance and exit of the crystal, was employed to handle the inherent trade-off of adiabatic process (Figure 1(b)). The RAP should ideally start and end near a stationary state where we can neglect the nonlinear coupling. We emphasize that the eigenstate at the exit of the crystal is quite different from that at the entrance. For SFG, all light is at the initial state, whereas at the final state, 40% of the light is at the third harmonic (Figure 1(c)). Meanwhile, the stationary state needs to vary very slowly by changing the phase mismatch in order to remain an eigenstate of the evolving system as it passes through the phase-matching (PM) concentration.

### 3. Experimental scheme and results

#### 3.1. SHG source architecture

The experimental setup is schematically shown in Figure 2(a). The pump source is a low-coherence broadband laser<sup>[33–36]</sup> that generates 4 ns pulses at 1058 nm, with an output energy of up to 500 mJ. After a 1:3 beam telescope, the diameter of the beam profile from the broadband pump source is 5 mm, and the input bandwidth (full width at half maximum (FWHM)) can reach 10 nm. The crystal temperature and incident angle are critical parameters that directly affect the efficiency and stability of nonlinear frequency conversion. A KDP crystal with a thickness of 18 mm, cut at  $\theta = 41.1^\circ$  and  $\varphi = 45^\circ$  for Type-I ( $o_{1w} + o_{1w} \rightarrow e_{2w}$ ) PM, is used in the SHG stage at room temperature

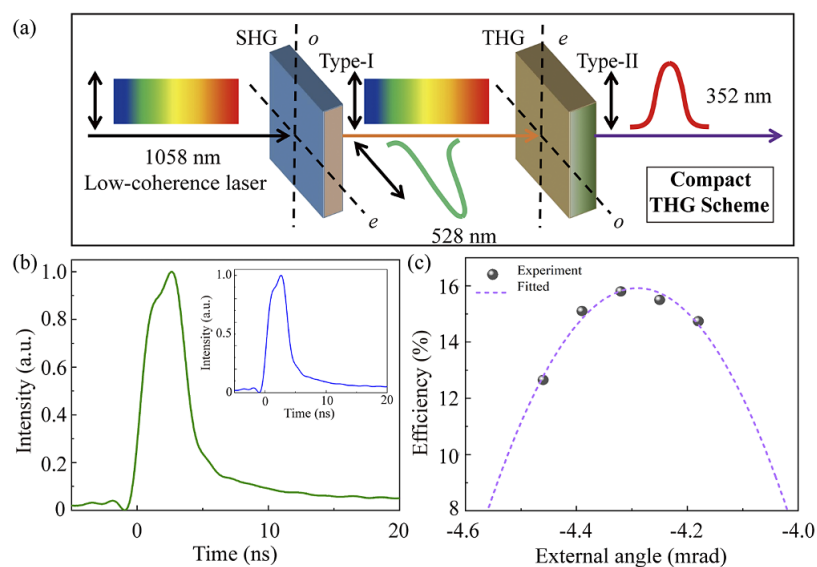


**Figure 2.** (a) Schematic setup of compact THG based on a low-coherence broadband laser. The optical axis of the SHG (THG) crystal is located in the horizontal (vertical) plane. (b) Pulse profile for SHG (green). Insert: pulse profile for the fundamental frequency (blue). (c) SHG efficiency is varied with the external angle (black dots) and its quadratic-polynomial fit (purple curve).

(note that all crystals employed in our experiment are equipped with anti-reflection coating for the corresponding wavelength). The effective nonlinear coefficient of KDP was  $d_{36}\sin\theta\sin2\varphi$  (Type-I) or  $d_{36}\sin2\theta\cos2\varphi$  (Type-II), where  $d_{36} = 0.38 \text{ pm/V}$ <sup>[37,38]</sup>.

Next, we reported the experimental results of SHG. The pulse profiles for SHG (green) and fundamental frequency (blue) are shown in Figure 2(b) and the insert. We demonstrated the conversion efficiency (Figure 2(c)) as a function of PM angle for Type-I SHG at a fundamental frequency energy of 40 mJ. The conversion efficiency for both SHG and THG, according to the Manley–Rowe relationship, is defined as the ratio of the generated pulse energy to total incident energy. We controlled the PM angle by a high-precision rotary stage where the minimum scale value is 0.02 mrad. The efficiency is very sensitive to the PM angle, which is tuned from  $-4.18$  to  $-4.46$  mrad, reaching a maximum efficiency of approximately 15.7% at  $-4.32$  mrad. We conducted the experiment of the generated spectrum under the largest SHG efficiency condition. After a KDP-based SHG stage, 90% of the energy corresponds to a bandwidth of approximately 5 nm with a central wavelength at 528.2 nm.

### 3.2. Compact THG configuration

We carried out a compact THG experiment under an output SHG pulse energy of 100 mJ, shown in Figure 2(a). The broadband SHG light output from the KDP crystal and the residual broadband fundamental light directly achieved the nonlinear frequency conversion process to generate the third harmonic. Different from SHG crystal, the optical axis of THG crystal is located in the vertical plane and we need to adjust the angle vertically. Only Type-II ( $e_{1w} + o_{2w} \rightarrow e_{3w}$ ) PM is studied for THG due to a slightly minimized group-velocity mismatch (GVM). When the angle of the controlled stage varied from 2.48 to 17.74 mrad, the conversion efficiency of the THG process was insensitive, which is due to the angular tolerance of the gradient deuterium DKDP crystal. As shown in Figure 3, the angle bandwidth (FWHM) is 15.26 mrad. Note that lower energy can avoid crystal damage and, at the same time, the efficiency is more sensitive to changes in the PM angle, making it easier to find the optimal angle. We fixed the angle at 10.5 mrad and changed the intensity of the input broadband fundamental light. The conversion efficiency of THG also varied and achieved a maximum THG conversion efficiency of approximately 7.16% when the fundamental frequency energy is about 400 mJ.

### 3.3. High-efficiency THG architecture

To enhance the efficiency of generating the broadband THG source, we combined the advanced broadband THG

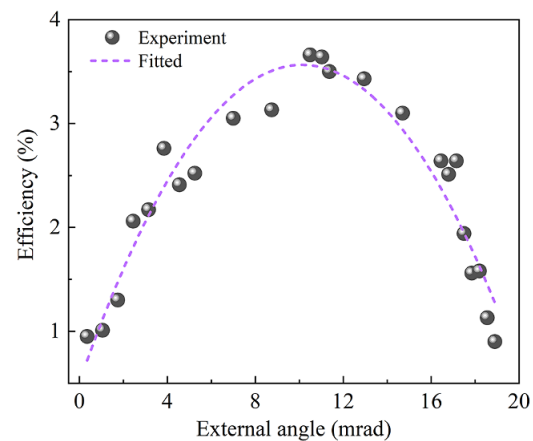


**Figure 3.** Dependence of tripling efficiency on the rotation angle of the gradient deuterium DKDP crystal (black dots) and its quadratic-polynomial fit (purple curve).

technology proposed by Liejia Qian with the adiabatic PM process<sup>[39–41]</sup>. It is an efficient frequency-tripling scheme for 352 nm broadband pulse generation by combination of broadband and narrowband Nd:glass lasers. This scheme eliminates the need for dispersive elements such as large-aperture gratings and can be combined with gradient deuterium DKDP crystal, potentially breaking through the trade-off in high efficiency and broad bandwidth. Research has found that using narrow-bandwidth laser pulses can slow down the GVM effect on efficiency during the nonlinear frequency conversion process of broadband lasers. Meanwhile, the GVM related to narrow-bandwidth lasers does not affect the PM bandwidth of THG, thereby scaling up the THG conversion efficiency of broadband lasers. Furthermore, by utilizing the large mismatch in group velocity for the Type-II PM process in KDP crystal, the introduction of narrow-bandwidth laser pulses during the THG process can effectively suppress the transfer of phase modulation of fundamental light to the intensity modulation of the generated frequency-tripling pulse, improving the uniformity and symmetry of the output beam profile.

The above-mentioned high-efficiency scheme for THG is shown in Figure 4. The broadband SHG source is introduced into the optical path of the THG stage after passing through a dichroic mirror (serving as a short-pass filter). The narrow-band fundamental light has a wavelength of 1064 nm, a pulse duration of 3 ns and an output energy of up to 2 J. In our experiment, a reference pulse serving as a time-synchronized benchmark is introduced. The leading edge of the narrow-band fundamental light pulse is first aligned with that of the reference pulse. Then, the pulse of the broadband frequency-doubled light is measured, and the delay is adjusted to align it with the leading edge of the reference pulse, thus achieving temporal synchronization. We measured the pulse profiles of both incident and reference beams by a photoelectric probe, as shown in the insert of Figure 4. The three front edges of the pulse profiles on the oscilloscope are in align-

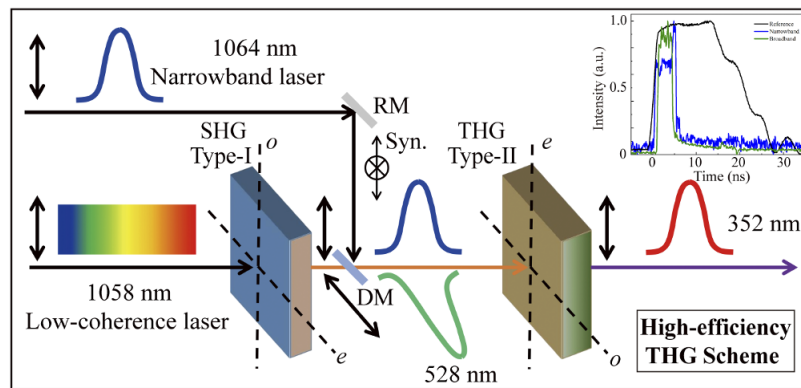


**Figure 4.** High-efficiency schematic diagram of THG through broadband and narrowband laser sources. The optical axis of the doubler (tripler) is also located in the horizontal (vertical) plane. Time synchronization of the broadband SHG pulse (green) and narrowband fundamental frequency pulse (blue) is maintained. DM, dichroic mirror; RM, reflection mirror; Syn., time synchronization. Insert: the black, blue and green solid lines represent the reference, narrowband and broadband pulses, respectively.

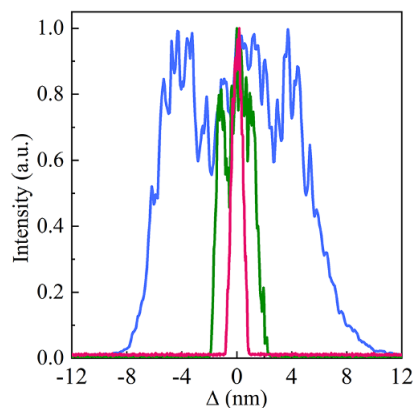


**Figure 5.** Measured spectra of fundamental frequency (blue), SHG (green) and THG (red) in the high-efficiency THG scheme. The spectra are centered at 1058, 528.2 and 352.1 nm, respectively.

ment, making the broadband frequency-doubled light and the narrowband fundamental light synchronously incident on the frequency-tripling crystal. A zeroth-order half-wave plate and a polarizer at Brewster's angle with respect to the incident light were adopted to continuously attenuate the narrow-bandwidth intensity. We can successively achieve the output energy of the narrow bandwidth through rotating the half-wave plate.

To enhance the efficiency of THG, it is essential to strictly ensure the spatial overlap of fundamental light and SHG light by precisely aligning their propagation directions. Furthermore, the conversion efficiency can also be improved if the beam aperture of the fundamental frequency light is slightly larger than that of SHG. After spatial coincidence and temporal synchronization of the two incident beams, a wide-bandwidth and narrow-bandwidth SFG process is realized in a gradient deuterium DKDP crystal for Type-II configuration. We obtain a broadband THG spectrum at the center wavelength of 352.1 nm with a bandwidth of about 4.4 THz (full width at  $1/e^2$  maximum), as shown in Figure 5.

Next, we demonstrate the angular robustness in our efficient frequency-tripling scheme. The energy of narrowband fundamental light was maintained at 100 mJ using an adjustable polarization system, while the energy for broadband SHG was kept at 50 mJ. When the gradient deuterium DKDP crystal was tuned, the frequency-tripling efficiency reached the maximum of about 22%. The efficiencies were also monitored when tuning the angle from  $-2.0$  to  $2.0$  mrad, all of which exceeded 10%. The angular bandwidth is 3.78 mrad (FWHM), as shown in Figure 6(a). In comparison, using a 36-mm-thickness KDP crystal for THG, the frequency-tripling efficiency reaches its maximum of approximately 14%. The angular bandwidth is 2.66 mrad at FWHM (Figure 6(b)). Both efficiency and angular bandwidth, obviously, were lower than those of gradient deuterium DKDP crystal. The high-efficiency frequency-tripling scheme utilizing gradient deuterium DKDP crystals exhibits angular robustness due to its adiabatic properties.

Gradient deuterium DKDP crystals can achieve efficient broadband THG output during the nonlinear frequency conversion process, achieving a conversion efficiency of 36.8% at  $0.15 \text{ GW/cm}^2$  using the RAP (Figure 7(a)). The energy of the narrowband pulse is fixed at 100 mJ in Figure 7 and the broadband pulse is 117 mJ when the conversion efficiency is 36.8%. In comparison to the compact THG configuration, the high-efficiency architectural design is capable of attaining a higher level of efficiency, partially due to the incorporation of a narrowband pulse. The conversion efficiency is observed to be in close proximity to the efficiency (approximately 40%) illustrated in Figure 1(c). This experimental discrepancy can be attributed to the losses incurred during the transmission of the light beam. When broadband and narrowband fundamental frequency lights are synchronously incident on a KDP crystal, broadband THG light is generated by traditional birefringent PM configuration. Figure 7 compares the adiabatic frequency conversion efficiency with that

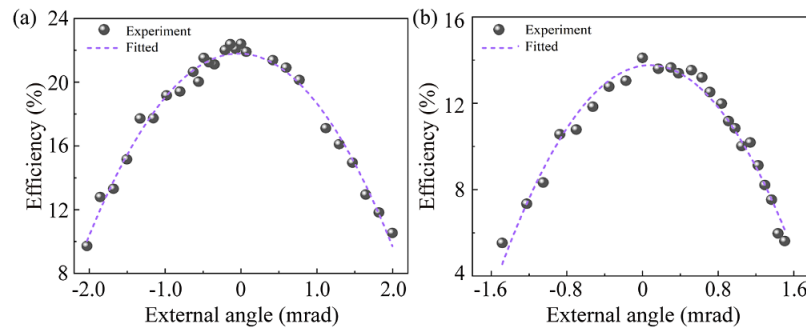


**Figure 6.** Conversion efficiency as a function of the crystal angular rotation for (a) gradient deuterium DKDP crystal and (b) KDP crystal. The experimental data (quadratic-polynomial fit) are represented by black dots (purple curve). The energy of narrowband and broadband pulses remained at 100 and 50 mJ, respectively.

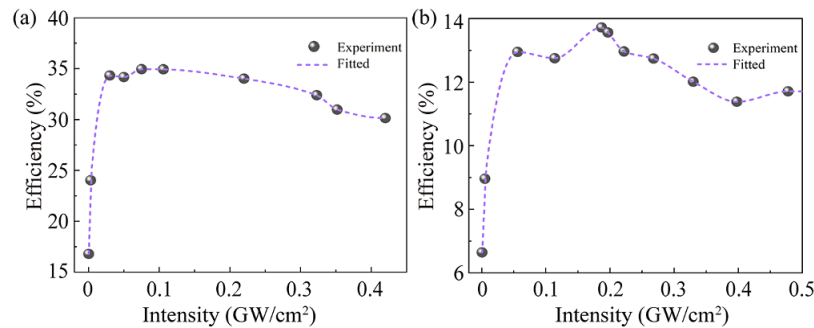


**Figure 7.** Measured efficiency as a function of broadband intensity at 1058 nm for (a) gradient deuterium DKDP crystal and (b) KDP crystal. Black dots and purple curve represent experimental data and the quadratic-polynomial fitted curve, respectively. The energy of the narrowband pulse is fixed at 100 mJ.

of the birefringent PM. The efficiency employed in the KDP is 13.7%, which is about one-third of the adiabatic frequency conversion (Figure 7(b)). With the increase of broadband intensity at 1058 nm, the efficiency of the RAP process decreases slowly and remains above 30%, while that of the birefringent PM decreases faster. Different performance of efficiency evolution indicates that, to achieve maximum efficiency, a smaller amount of intensity is required in the RAP process. After reaching the optimal efficiency, further increasing the injection leads to an increase of tripling energy in both the RAP process and birefringent PM, but there was no significant decrease in the efficiency of the RAP method.

Compared to the two-crystal cascade scheme (1.1 THz @351 nm) proposed by Eimerl *et al.*<sup>[5]</sup> and Babushkin *et al.*<sup>[6]</sup>, we obtained a broader bandwidth of 4.4 THz. In comparison with the novel method using grating angular dispersion compensation with an efficiency of approximately 8% (in the proof-of-concept experiment)<sup>[7]</sup>, limited by the damage threshold of ultraviolet gratings and the beam overlap, our method can be applied to high-energy pulses while maintaining high efficiency (about 36.8%). Furthermore, we would like to emphasize that there is still potential for improvement in the efficiency of our experimental scheme. As the gradient deuterium DKDP crystal was newly reported in 2023, only one crystal is currently available for the THG process. In the future,

crystals tailored for the frequency doubler and tripler will be employed, and the adiabatic process will be applied in the entire scheme, which is expected to significantly improve efficiency and bring it close to the quantum limit.

#### 4. Conclusion

In summary, we have demonstrated the generation of THG in gradient deuterium DKDP crystals by the RAP process. We have developed a compact THG setup that can obtain 352 nm pulses with a bandwidth of 4.4 THz, achieving an efficiency of 7%. By introducing a narrowband fundamental laser, the efficiency can be scaled up to 36%. Compared to KDP crystal, gradient deuterium DKDP crystal is a better potential candidate to generate THG due to the robustness of the RAP process. The gradient deuterium DKDP combined with RAP is easy to implement and the doping profile can be reconfigured for different design parameters. Furthermore, we believe that these results are very helpful for the development of high-efficiency and broadband lasers based on gradient-doped crystals.

#### Acknowledgements

This work was supported by the President Funding Independent Project of the China Academy of Engineering Physics (No. YZJJZL2024200), the National Natural

Science Foundation of China (No. 62405298) and the National Key Research and Development Program of China (No. 2023YFA1608503). The authors thank Mingxia Xu and Xun Sun of Shandong University for the discussion about gradient deuterium DKDP crystals.

## References

1. S. P. Obenshain, N. C. Luhmann Jr, and P. T. Greiling, *Phys. Rev. Lett.* **36**, 1309 (1976).
2. R. Betti and O. A. Hurricane, *Nat. Phys.* **12**, 435 (2016).
3. Y. Chen, X. Zhu, S. Ma, H. Yu, H. Wu, Z. Hu, and Y. Wu, *Opt. Mater. Express* **13**, 3164 (2023).
4. J. Zhao, H. Lu, J. Zheng, D. Li, Y. Zhang, X. Gan, and J. Zhao, *Opt. Lett.* **49**, 3130 (2024).
5. D. Eimerl, J. M. Auerbach, C. E. Barker, D. Milam, and P. W. Milonni, *Opt. Lett.* **22**, 1208 (1997).
6. A. Babushkin, R. S. Craxton, S. Oskoui, M. J. Guardalben, R. L. Keck, and W. Seka, *Opt. Lett.* **23**, 927 (1998).
7. C. Dorrer, M. Spilatro, S. Herman, T. Borger, and E. M. Hill, *Opt. Express* **29**, 16135 (2021).
8. H. Suchowski, D. Oron, A. Arie, and Y. Silberberg, *Phys. Rev. A* **78**, 063821 (2008).
9. H. Suchowski, V. Prabhudesai, D. Oron, A. Arie, and Y. Silberberg, *Opt. Express* **17**, 12731 (2009).
10. R. P. Feynman, F. L. Vernon Jr, and R. W. Hellwarth, *J. Appl. Phys.* **28**, 49 (1957).
11. Y. Ban, L. Jiang, Y. Li, L. Wang, and X. Chen, *Opt. Express* **26**, 31137 (2018).
12. A. Ramachandran, J. Fraser-Leach, S. O'Neal, D. G. Deppe, and K. C. Hall, *Opt. Express* **29**, 41766 (2021).
13. L. Allen and J. H. Eberly, *Optical Resonance and Two Level Atoms* (Dover, New York, 1987).
14. J. Moses, H. Suchowski, and F. X. Kärtner, *Opt. Lett.* **37**, 1589 (2012).
15. E. Bahar, X. Ding, A. Dahan, H. Suchowski, and J. Moses, *Opt. Express* **26**, 25582 (2018).
16. H. Suchowski, G. Porat, and A. Arie, *Laser Photonics Rev.* **8**, 333 (2014).
17. A. Markov, A. Mazhorova, H. Breitenborn, A. Bruhacs, M. Clerici, D. Modotto, O. Jedrkiewicz, P. Trapani, A. Major, F. Vidal, and R. Morandotti, *Opt. Express* **26**, 4448 (2018).
18. X. Liu, X. J. Shen, T. Rui, L. He, B. Zhou, and N. Zheng, *Opt. Lett.* **45**, 467 (2020).
19. P. Zhang, J. Cheng, Y. Wu, R. Yan, R. Zhu, T. Wang, L. Jiang, C. Tong, and Y. Song, *Opt. Express* **32**, 5011 (2024).
20. E. Simonova, A. Kokh, V. Shevchenko, A. Kuznetsov, A. Kragzhda, and P. Fedorov, *Crystal Res. Technol.* **54**, 1800267 (2019).
21. R. Murai, T. Fukuhara, G. Ando, Y. Tanaka, Y. Takahashi, K. Matsumoto, H. Adachi, M. Maruyama, M. Imanishi, K. Kato, M. Nakajima, Y. Mori, and M. Yoshimura, *Appl. Phys. Express* **12**, 075501 (2019).
22. Y. Orii, K. Kohno, H. Tanaka, M. Yoshimura, Y. Mori, J. Nishimae, and K. Shibuya, *Opt. Express* **30**, 11797 (2022).
23. Z. Hu, Y. Zhao, Y. Yue, and X. Yu, *J. Crystal Growth* **335**, 133 (2011).
24. N. Wang, J. Zhang, H. Yu, X. Lin, and G. Yang, *Opt. Express* **30**, 5700 (2022).
25. H. Yuan, Y. Li, Z. Dan, S. Zhang, and C. Zhu, *Opt. Express* **31**, 35786 (2023).
26. Z. Cui, L. Han, C. Wang, M. Sun, D. Liu, and J. Zhu, *Opt. Lett.* **47**, 2947 (2022).
27. H. Qi, Z. Wang, F. Yu, X. Sun, X. Xu, and X. Zhao, *Opt. Lett.* **41**, 5823 (2016).
28. H. Yang, D. Li, C. Song, and W. Cheng, *Opt. Laser Technol.* **141**, 107105 (2021).
29. G. Hao, M. Xu, X. Sun, B. Liu, L. Zhang, H. Ren, J. Bai, and J. Gao, *Crystal Growth Design* **24**, 567 (2023).
30. G. Porat and A. Arie, *J. Opt. Soc. Am. B* **30**, 1342 (2013).
31. H. Suchowski, B. D. Bruner, A. Ganany-Padowicz, I. Juwiler, A. Arie, and Y. Silberberg, *Appl. Phys. B* **105**, 697 (2011).
32. H. Suchowski, P. R. Krogen, S. W. Huang, F. X. Kärtner, and J. Moses, *Opt. Express* **21**, 28892 (2013).
33. L. Ji, X. Zhao, D. Liu, Y. Gao, Y. Cui, D. Rao, W. Feng, F. Li, H. Shi, J. Liu, X. Li, L. Xia, T. Wang, J. Liu, P. Du, X. Sun, W. Ma, Z. Sui, and X. Chen, *Opt. Lett.* **44**, 4359 (2019).
34. Y. Cui, Y. Gao, D. Rao, D. Liu, F. Li, L. Ji, H. Shi, J. Liu, X. Zhao, W. Feng, L. Xia, J. Liu, X. Li, T. Wang, W. Ma, and Z. Sui, *Opt. Lett.* **44**, 2859 (2019).
35. X. Zhao, L. Ji, D. Liu, Y. Gao, D. Rao, Y. Cui, W. Feng, F. Li, H. Shi, C. Shan, W. Ma, and Z. Sui, *Appl. Phys. Lett.* **5**, 091301 (2020).
36. Z. Sui and K. Lan, *Matter Radiat. Extremes* **9**, 4 (2024).
37. J. E. Midwinter and J. Warner, *Br. J. Appl. Phys.* **16**, 1135 (1965).
38. I. Shoji, T. Kondo, A. Kitamoto, M. Shirane, and R. Ito, *J. Opt. Soc. Am. B* **14**, 2268 (1997).
39. Y. Chen, P. Yuan, L. Qian, H. Zhu, and D. Fan, *Opt. Commun.* **283**, 2737 (2010).
40. H. Zhong, P. Yuan, S. Wen, and L. Qian, *Opt. Express* **22**, 4267 (2014).
41. Y. Chen, P. Yuan, and L. Qian, *J. Opt.* **13**, 075205 (2011).